I&EC research
Industrial & Engineering Chemistry Research

Article

Cite This: Ind. Eng. Chem. Res. 2019, 58, 19503−19510

pubs.acs.org/IECR

Manipulating Oxidation States of Copper within Cu-BTC Using $Na_2S_2O_3$ as a New Strategy for Enhanced Adsorption of Sulfide

Dan Wang,[†] Hao Jiang,[†] Jialun Tan,[†] Yuxiang Chen,[†] Yang An,[†] Yonghao Chen,[†] Yuan Wu,[†] Chuanlei Liu,[†] Hui Sun,*[,†,‡] Jichang Liu,[†,‡] Di Wu,*[,§,∥,⊥,#] and Benxian Shen[†]

[†]Petroleum Processing Research Center and [‡]International Joint Research Center of Green Energy Chemical Engineering, East China University of Science and Technology, Shanghai 200237, China

[§]Alexandra Navrotsky Institute for Experimental Thermodynamics, [∥]The Gene and Linda Voiland School of Chemical Engineering and Bioengineering, [⊥]Materials Science and Engineering, and [#]Department of Chemistry, Washington State University, Pullman, Washington 99163, United States

Supporting Information

ABSTRACT: Manipulation of the oxidation states of the metal species within metal−organic frameworks leads to compositional, structural, and surface property evolutions, which will impact their performance as sorbents in adsorptive separation processes. In this study, we propose a new low-cost postsynthesis strategy to modify the oxidation states of copper species within the copper-1,3,5-benzenetricarboxylic acid (Cu-BTC) structure employing $Na_2S_2O_3$ as the reducing agent. The compositional and structural evolutions of the modified samples were thoroughly characterized by a series of methods, and the dimethyl disulfide (DMDS) adsorption performance was evaluated. Accurately controlled reduction of Cu(II) to Cu(I) and formation of nanopores in the modified Cu(I)/Cu(II)-BTC samples have been observed and confirmed experimentally. Specifically, the sample 0.46/Cu-BTC/24h with a Cu(I)/Cu(II) molar ratio of 1.79 exhibits both the highest DMDS adsorption capacity (146.66 mg-S/g) and fastest diffusion with D of 7.59×10^{-13} cm^2/s at 298 K. Further density functional theory calculations reveal that the modified Cu(I)/Cu(II)-BTC structures exhibit much higher interaction energy, E_{in}, with DMDS (70.65 kJ/mol) than the parent Cu(II)-BTC (20.28 kJ/mol). Controllable reduction of Cu(II) to Cu(I) in Cu-BTC leads to significantly enhanced guest−host interactions as well as the formation of uniform nanoscale porosity leading to effect enhancement for the adsorption of DMDS using modified Cu-BTC materials.

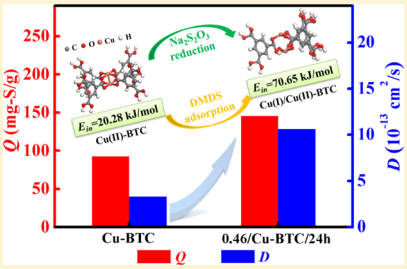

1. INTRODUCTION

Sulfur compounds contained in petroleum reduce the quality of oil products, cause serious corrosion of process pipelines and storage equipment, and lead to serious emission of SO_x, one the main air pollutants. Therefore, the sulfur species in the petroleum products has to be strictly controlled according to the regulation standards.[1−4] Generally, a family of sulfur compounds is present in light petroleum products, including hydrogen sulfide, mercaptan, thioether, disulfide, and carbonyl sulfide. Compared with other sulfides, disulfides are very challenging to be separated with low removal efficiency in typical desulfurization processes because of their lower reactivity, dissolving activity, and adsorption affinity. Significant efforts have been made to enable selective removal of disulfides such as dimethyl disulfide (DMDS).[5]

Typically, the commonly applied desulfurization strategies include hydrodesulfurization,[6] oxidative desulfurization,[7,8] biological desulfurization,[9,10] extraction desulfurization,[11] adsorption desulfurization (ADS),[12] and so on. Among all these methods, ADS is very promising owing to its remarkable advantages, such as relatively low-cost, mild operating conditions, straightforward process design, and consistent reproducibility.[13,14] Qualified adsorbents with great performance are expected to have large specific surface area and pore volume, suitable pore structure, and abundant adsorption active sites.

During the past decades, various porous materials including zeolite molecular sieves, silica, carbon-based adsorbents, and active alumina[15−17] were evaluated as desulfurization sorbents. Recently, metal−organic frameworks (MOFs) have shown promising performance as adsorbents in many applications because of their well-defined framework configuration, large surface area, and tunable pore characteristics.[18,19] Specifically, copper-1,3,5-benzenetricarboxylic acid (Cu-BTC) has been demonstrated to exhibit high adsorption capacity for sulfur compounds owing to its dense coordinatively unsaturated metal active sites. Essentially, adsorption of sulfides on Cu-BTC is enabled by the S−M bond formation during guest−host interactions between the sulfide molecules and the Cu-BTC framework structure.[20] According to Pearson's hard and soft acid−base theory, disulfides and mercaptans (as soft Lewis bases) are tightly bonded to metal ions (such as Cu(II), Cu(I)), which act as soft Lewis acids.[21] In addition, π-

Received: August 7, 2019
Revised: September 27, 2019
Accepted: September 27, 2019
Published: September 27, 2019

DOI: 10.1021/acs.iecr.9b04349
Ind. Eng. Chem. Res. 2019, 58, 19503−19510

complexation is another extensively used mechanism to explain the adsorption affinity of sulfide molecules to Cu-coordinated structures.[22] Besides, a synchronizing integration of porosity or pore size with the specific adsorption sites of Cu-BTC will simultaneously promote sulfur compound removal with enhanced efficiency.[23−25] Significant efforts have been made to tune the pore structure and metal sites to improve the ADS performance. Notably, Fan et al. synthesized a Cu-BTC/activated carbon composite with better performance for removal of hydrogen sulfide and DMDS compared with the pristine Cu-BTC. Improved adsorption performance was ascribed to the larger pore volume and more copper metal sites in the composite structure.[23] Du et al. modified Cu-BTC via incorporating attapulgite and obtained a markedly improved adsorption performance for DMDS owing to more efficient utilization of active sites as well as larger surface area enabled by the modified Cu-BTC particles.[26]

Recently, we reported that modified Cu(I)/Cu(II)-BTC structures showed significantly enhanced adsorption affinity toward small organosulfur compounds. Specifically, we reduced the some of the Cu(II) to Cu(I) within the Cu-BTC structure using ethanol (EtOH) as the reducing agent and employing impregnated Ag as the catalyst.[27] However, economically, this modified sorbent is expensive including precious metal (Ag), and the preparation process is complicated involving multichemical modification. Herein, we report a new strategy to harness the redox reaction between Cu species within the Cu-BTC framework and $Na_2S_2O_3$ for reduction of Cu(II) to Cu(I) in the Cu-BTC structure. We thoroughly characterized these modified samples using a spectrum of techniques. We also evaluated the DMDS adsorption performance, from the perspective of both capacity and diffusion. Moreover, density functional theory (DFT) calculations were performed to generate comprehensive models and quantify the energies of interactions between DMDS and two MOF structures.

2. EXPERIMENTAL SECTION

2.1. Chemicals. Copper nitrate ($Cu(NO_3)_2{\cdot}3H_2O$, >99%) and 1,3,5-benzenetricarboxylic acid (H_3BTC, >98.0%) were provided by Shanghai Macklin Biochemical Co., Ltd. *N*,*N*-Dimethylformamide (>99.5%), normal hexane (>99.5%), ethanol (>99.5%), and sodium thiosulfate pentahydrate ($Na_2S_2O_3{\cdot}5H_2O$, >99.0%) were purchased from Shanghai Titan Scientific Co., Ltd. DMDS (>98.0%) was obtained from Tokyo Chemical Industry Co., Ltd. All of the chemicals were directly utilized without any further purification.

2.2. Preparation of Samples. Cu-BTC samples were prepared according to the procedure described in our previous publication.[27] A series of modifications on Cu-BTC were conducted in the presence of $Na_2S_2O_3$ to achieve controllable reduction of Cu(II) to Cu(I). Synthesized Cu-BTC sample (2 g) was immersed in 100 mL of $EtOH/H_2O$ solution (ethanol to H_2O volume ratio of 1:1) containing $Na_2S_2O_3$. Subsequently, the suspension was put in an aforementioned autoclave and kept at 358 K for given time. $EtOH/H_2O$ solutions with different $Na_2S_2O_3$ concentrations were used to control starting S/Cu molar ratios from 0 up to 2 while reduction time was increased regularly from 0 to 24 h. Employing the same washing and drying procedures as we used in Cu-BTC synthesis, cyan solid powder was obtained. The samples were labeled as *x*/Cu-BTC/*y*, in which *x* is the starting S/Cu molar ratio utilized for each postsynthesis and *y* is the reduction time.

2.3. Characterizations. The surface morphology features of all samples were examined by using a NOVA Nano SEM450 scanning electron microscope (SEM; FEI, USA) with a beam current of 10 nA and accelerating voltage of 15 kV.

X-ray powder diffraction (XRD) analyses were performed by using a Bruker D8 Advance diffractometer (Bruker AXS Inc., Germany) with Cu Kα radiation operated at 40 kV and 40 mA. All data were obtained using the 2θ range from 5° to 75° with 0.02° interval.

Fourier transform infrared (FTIR) spectroscopy analyses were determined on a Nicolet 6700 FTIR spectrometer (Thermo Fisher Scientific, USA) applying a KBr tablet.

Raman spectra were collected using a Renishaw inVia Reflex Raman microscope and spectrometer (Renishaw Plc., U.K.) equipped with an argon ion laser at a wavelength of 514 nm. A grating of 2400 lines/mm was used to examine the configurations between metal ions and organic ligands, providing a spectral resolution of 1.14 cm^{-1}.

X-ray photoelectron spectroscopy (XPS) measurements were conducted with an ESCALAB 250Xi spectrometer (Thermo Fisher Scientific, USA) equipped with Al Kα radiation as a X-ray source (14 kV, 250 W). The binding energies of all samples were corrected by calibrating the C 1s peak at 284.6 eV. Detailed valence states and content of Cu species in Cu-BTC samples were confirmed through fitting the XPS spectra using XPSPEAK software.[28]

Pore structure analyses were performed by N_2 adsorption at 77 K using a Micromeritics ASAP 2020 V4.00 (Micromeritics, Norcross GA). Specific surface area and pore volume were calculated using the Brunauer−Emmett−Teller and the Horvath−Kawazoe method, respectively. All samples were degassed at 423 K for 12 h prior to measurement.

2.4. Adsorption Capacity Measurements. Adsorption capacities of the Cu-BTC samples were evaluated according to the methods previously reported.[27] Here, we select DMDS, which is commonly contained in light hydrocarbons, as the probe sulfur compound. All adsorption measurements were performed at 293 K. Adsorption capacities for DMDS, *Q* (mg-S/g—adsorbent) are calculated from the initial and equilibrated concentrations of DMDS in the liquid phase according to eq 1.

$$Q = w(c_0 - c)/m \times 10^{-3} \tag{1}$$

where *w* and *m* are the masses of the model oil and adsorbent (g), respectively; c_0 and *c* are the initial and equilibrium concentrations of DMDS in liquid phase (μg-S/g), respectively.

2.5. Adsorption Kinetics Measurements. The adsorption uptake curves were recorded to determine the rate of DMDS adsorption on the parent and modified Cu-BTC samples. Adsorption tests were performed at three different temperatures, 288, 298, and 308 K. For each test, the concentrations of DMDS in liquid phase were determined at given time intervals to construct the adsorption uptake curve. Furthermore, a simplified expression[29] (see eq 2) was used to elucidate the obtained adsorption uptake curves for the parent and modified Cu-BTC samples.

$$\frac{q_t}{q_e} = 1 - \frac{6}{\pi^2}\sum_{n=1}^{\infty}\frac{1}{n^2}\exp\left(-\frac{n^2\pi^2 Dt}{r^2}\right) \tag{2}$$

DOI: 10.1021/acs.iecr.9b04349
Ind. Eng. Chem. Res. 2019, 58, 19503−19510

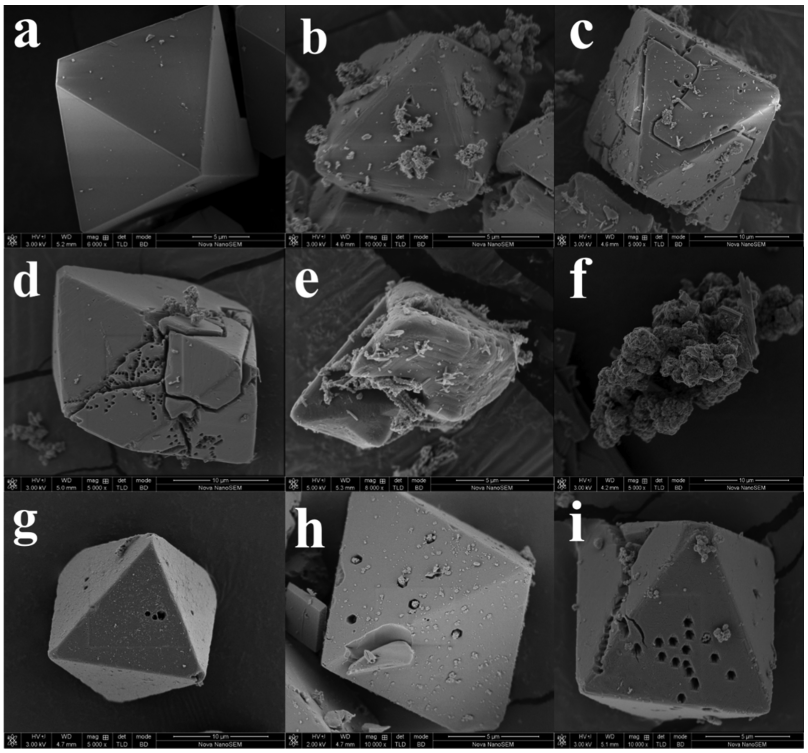

Figure 1. SEM images of (a) Cu-BTC, (b) 0.3/Cu-BTC/24h, (c) 0.46/Cu-BTC/24h, (d) 0.5/Cu-BTC/24h, (e) 1/Cu-BTC/24h, (f) 2/Cu-BTC/24h, (g) 0.46/Cu-BTC/1h, (h) 0.46/Cu-BTC/6h, and (i) 0.46/Cu-BTC/12h samples.

in which D/r^2 is the apparent diffusion time constant of the adsorbate molecules in the crystal particle, s^{-1}. r represents the crystal radius, cm, and is found to be 0.50×10^{-3} cm from the SEM characterizations (see Figure 1). D is the diffusion coefficient, cm^2/s. t represents the adsorption time, s. q_t and q_e are adsorption amounts for DMDS at adsorption time t and the time reaching adsorption equilibrium, respectively, with the unit mg-S/g.

2.6. DFT Calculations. DFT calculations were performed using Dmol3 program[30] in Materials Studio 6.1 package. Perdew–Burke–Ernzerhof function with high accuracy in generalized gradient approximation[31] was used as the exchange correlation function for all calculations. DFT semicore pseudopods calculations were performed with double numerical basis sets plus polarization function. A quality module is set to be customized. Geometric optimization based on convergence of force, displacement, and energy is performed without any symmetry restriction and the convergence tolerance value for geometry optimization is presented in Table S1.

Interaction energy E_{in} of DMDS adsorption on different Cu-BTC structures is defined as the difference between total energy of DMDS molecule guest and Cu-BTC structure host before adsorption and energy of interacted guest–host system. It is directly calculated by eq 3.

$$E_{in} = E_{(adsorbate+adsorbent)} - E_{(adsorbate)} - E_{(adsorbent)} \quad (3)$$

where $E_{(adsorbate+adsorbent)}$ is the energy of guest–host system, eV. $E_{(adsorbate)}$ is the energy of DMDS molecule, eV. $E_{(adsorbent)}$ is the energy of free surface of adsorbent Cu-BTC, eV. The negative interaction energy suggests an energetically favorable exothermic interaction.

3. RESULTS AND DISCUSSION

3.1. Characterizations of Samples. A series of modified Cu-BTC products were synthesized under different postsynthesis conditions detailed in Table S2.

The SEM image of the parent Cu-BTC illustrates a well-defined octahedron morphology with sharp triangular faces and an average diameter of 10 μm (Figure 1a). Upon further modification, the crystal surface becomes rough and shows clearly identified nanoscale pores with uniform size around 100 nm. As the $n(S)/n(Cu)$ ratio increases, the roughness of the crystal surface increases accordingly (see Figure 1a–f). The crystals of samples with large $n(S)/n(Cu)$ ratios, including 1/Cu-BTC/24h with $n(S)/n(Cu)$ of 1 (see Figure 1e) and 2/Cu-BTC/24h with $n(S)/n(Cu) = 2$ (see Figure 1f), are found to suffer from severe structural destruction or even collapse. In addition, when $n(S)/n(Cu) = 0.46$, the number of nanopores on the crystal surfaces of modified samples tends to increase as the reduction time increases (Figure 1c,g–i). Therefore, these SEM images suggest that the nanoscale porosity, which is considered to enable faster DMDS diffusion rate into the internal porous structures of Cu-BTC, can be tuned via reduction time control.

To identify the crystallinity and phase of all samples, XRD analyses were conducted on the parent and modified Cu-BTC samples (Figures 2 and 3). The parent sample shows the typical XRD peaks of Cu-BTC, which can be indexed to a cubic crystalline copper trimesate trihydrate (JCPDS card no. 00-062-1183).[32] Additionally, other than 2/Cu-BTC/24h, all modified samples exhibit similar diffraction patterns as that of the parent sample. Moreover, a characteristic peak at 11.79° [referring to (222) reflection plane] shows increased intensity as the $Na_2S_2O_3$ dosage in the starting postsynthesis system or the reduction time increases (see Figures 2 and 3). Unlike

DOI: 10.1021/acs.iecr.9b04349
Ind. Eng. Chem. Res. 2019, 58, 19503–19510

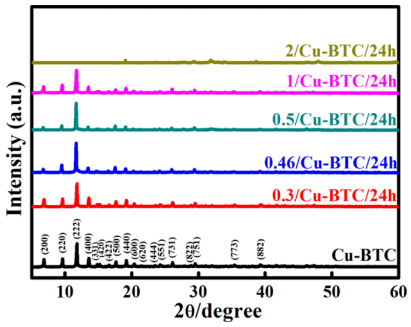

Figure 2. XRD patterns of different Cu-BTC samples modified with different $Na_2S_2O_3$ dosages.

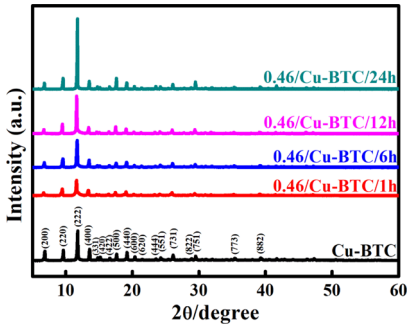

Figure 3. XRD patterns of different Cu-BTC samples modified with different reduction times.

other samples with different $n(S)/n(Cu)$, 2/Cu-BTC/24h nearly lost all of the characteristic peaks of Cu-BTC, indicating that the excessive $Na_2S_2O_3$ leads to complete structure collapse of the Cu-BTC framework. This phenomenon is in good agreement with and supported by the SEM images we observed in this study. Thus, the dosage of $Na_2S_2O_3$ needs to be accurately controlled within an appropriate range in the postsynthesis process to avoid undesirable damage to the Cu-BTC framework.

Additionally, FTIR and Raman spectroscopy analyses were conducted to examine the bonding and structural evolutions upon modification. All samples show quite similar characteristic peaks in the FTIR spectra (see Figure 4). An absorption peak appearing at 3444.6 cm^{-1} is attributed to O−H stretching vibration from water molecules which are not completely desorbed through the drying process.[33] The peak at 1637.8 cm^{-1} is related to C═O stretching vibration of free carboxylic acid because of bimolecular association in the carboxylic acid

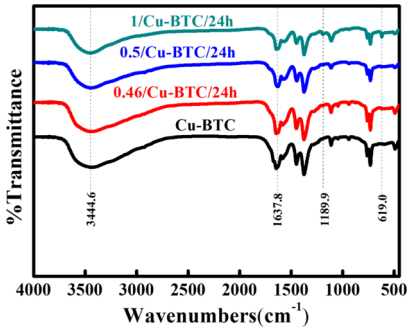

Figure 4. FTIR spectra of different Cu-BTC samples modified with different $Na_2S_2O_3$ dosages.

molecules.[34] For the spectra of modified samples, two new peaks are observed at 1189.9 and 619.0 cm^{-1}, which correspond to C−O (ring) stretching vibration of carbohydrates[35] and Cu−O vibration mode,[36] respectively.

For the Raman spectrum of Cu-BTC (see Figure 5), the C═C vibration modes of benzene ring can be recognized from

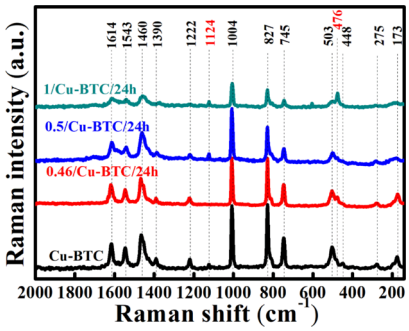

Figure 5. Raman spectra of different Cu-BTC samples modified with different $Na_2S_2O_3$ dosages.

the peaks located at 1614 and 1004 cm^{-1}.[37] The doublet at 1543 and 1460 cm^{-1} indicates the O−C−O asymmetrical and symmetrical stretching vibrations, respectively. Bands at 827 and 745 cm^{-1} are related to out-of-plane bending vibrations of C−H in rings. Moreover, the three peaks at 275, 448, and 503 cm^{-1} are ascribed to Cu(II)−O vibrations of the O atoms in the carboxylate bridges.[38] Bands located at 1390 and 1220 cm^{-1} can be assigned to in-plane bending vibration of C−H in aldehyde groups and symmetric stretching vibration of C−O−C. At last, peaks at 170−195 cm^{-1} correspond to Cu−Cu stretching modes. On the other hand, for the three modified samples, structural evolutions can be identified from the Raman spectra. 0.46/Cu-BTC/24h exhibits very consistent Raman spectrum with the parent Cu-BTC, indicating a well-preserved framework. As the dosage of reducing agent increases, the modified samples (0.5/Cu-BTC/24h and 1/Cu-BTC/24h) show gradually decreased peak at 173 cm^{-1}, suggesting the breakage of Cu−Cu bonds. A series of changes at 275, 448, and 503 cm^{-1} correspond to the evolution of Cu−O vibrations because of the reduction of Cu species from Cu(II) to Cu(I). In addition, a new peak located at 476 cm^{-1} appears in the spectrum of 1/Cu-BTC/24h, a strong indication of the corresponding oxidized species of $S_2O_3^{2-}$.[39] Hence, the evolving Raman spectra highlight the structural evolutions of Cu-BTC after postsynthesis modification.

To further confirm the reduction of Cu(II) to Cu(I) for Cu-BTC with different $Na_2S_2O_3$ dosages, the Cu species of the original and modified Cu-BTC samples were characterized by XPS analysis (see Figure 6). The binding energy was corrected by using the C 1s peak at 284.6 eV as a reference. Specifically, the parent and modified Cu-BTC samples all present a peak centered at about 935.0 eV (ranging from 934.6 to 935.0 eV), which corresponds to Cu(II) $2p_{3/2}$.[40] The spectrum of each modified sample features an additional Cu(I) $2p_{3/2}$ peak ranging from 932.5 to 933.2 eV accompanied with a decreased Cu(II) $2p_{3/2}$ peak intensity compared with the original sample. All Cu species within the parent Cu-BTC are confirmed to be Cu(II), whereas in the modified Cu-BTC samples both Cu(I) and Cu(II) species are detected. This is a strong evidence demonstrating the successful reduction of Cu(II) to Cu(I) with $Na_2S_2O_3$. Additionally, the Cu(I)/Cu(II) molar ratios for

DOI: 10.1021/acs.iecr.9b04349
Ind. Eng. Chem. Res. 2019, 58, 19503−19510

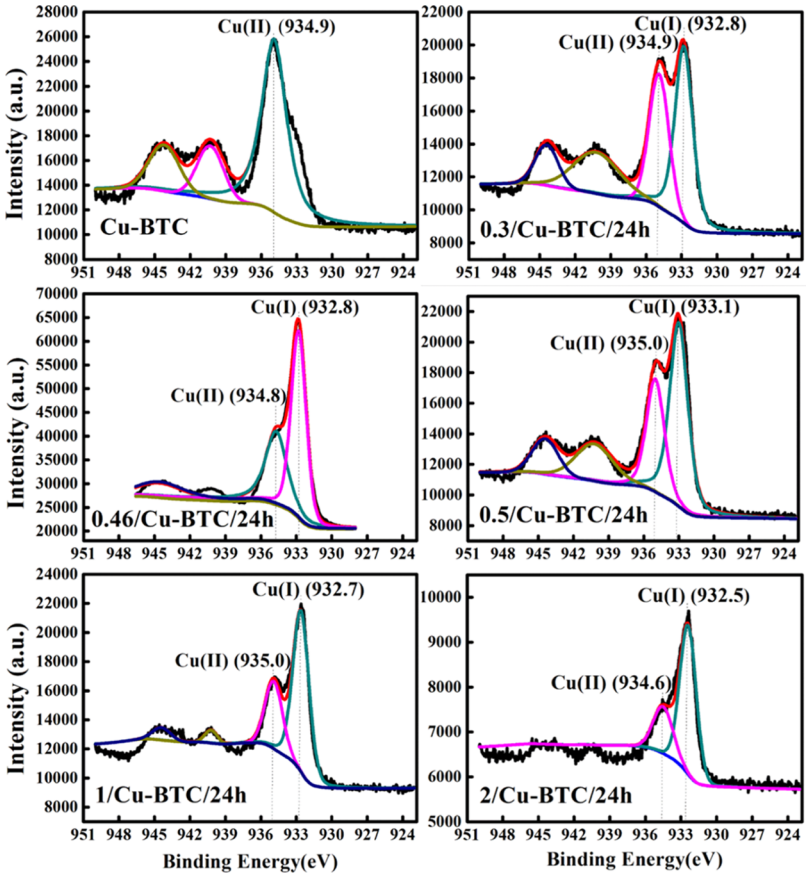

Figure 6. Cu $2p_{3/2}$ XPS spectra of different Cu-BTC samples modified with different $Na_2S_2O_3$ dosages.

all samples are determined by integration of the XPS peaks (see Table S3). The XPS results suggest that the modified Cu-BTC samples have monotonically increased Cu(I)/Cu(II) molar ratios as the dosage of $Na_2S_2O_3$ increases. Moreover, these XPS results suggest that the metal compositions of Cu-BTC can be accurately modified via simply control in the dosage of $Na_2S_2O_3$. This strategy can be employed to enhance the DMDS adsorption.

3.2. DMDS Adsorption Enhancement on Modified Cu-BTC. Batch adsorption experiments were conducted at room temperature to investigate the effects of $Na_2S_2O_3$ modification on sulfide adsorption performance of Cu-BTC. The model oil has an initial DMDS concentration of 2500 μg-S/g. As shown in Figure 7, as the S/Cu molar ratio increases, the two modified Cu-BTC samples, 0.3/Cu-BTC/24h and 0.46/Cu-BTC/24h, demonstrate significantly enhanced DMDS adsorption capacities, from 89.23 mg-S/g for the parent Cu-BTC to 137.41 mg-S/g for 0.3/Cu-BTC/24h, and 146.66 mg-S/g for 0.46/Cu-BTC/24h. However, we also find that the DMDS adsorption capacity of 2/Cu-BTC/24h (17.81 mg-S/g) does not follow the same increasing trend as other modified samples as the n(S)/n(Cu) ratio increases. This is caused by the serious destruction to the Cu-BTC structure because of the excessive $Na_2S_2O_3$ dosage (see Figure 1e,f). On the other hand, as the reduction time increases, the DMDS adsorption capacity exhibits a monotonically ascending trend (see Figure 8). To further determine the effect of controllable reduction on DMDS adsorption quantitatively, the adsorption capacity is plotted against the Cu(I)/Cu(II) molar ratio (see Figure 9). Specifically, as the Cu(I)/Cu(II) ratio increases, the

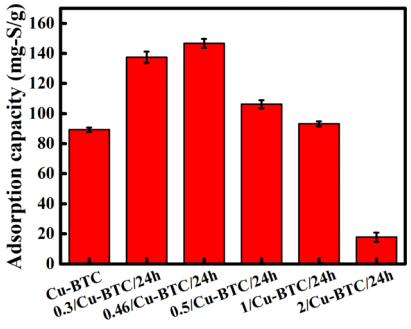

Figure 7. Adsorption capacities of DMDS on Cu-BTC samples modified with different $Na_2S_2O_3$ dosages.

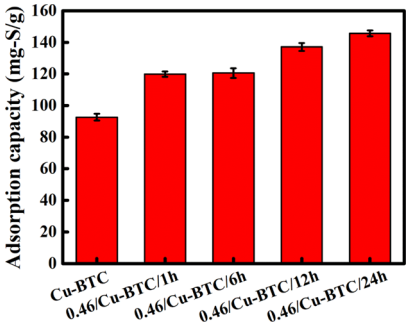

Figure 8. Adsorption capacities of DMDS on Cu-BTC samples modified with different reduction timse.

DOI: 10.1021/acs.iecr.9b04349
Ind. Eng. Chem. Res. 2019, 58, 19503−19510

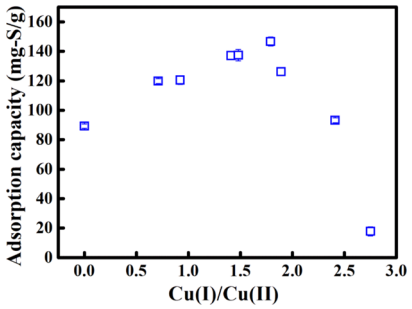

Figure 9. Relationship between DMDS adsorption capacities (Q) and Cu(I)/Cu(II) molar ratios of Cu-BTC samples.

initially increasing DMDS adsorption capacity levels at a plateaus at Cu(I)/Cu(II) = 1.79, followed by an abrupt decrease at Cu(I)/Cu(II) = 2.75 reaching 17.81 mg-S/g for 2/Cu-BTC/24h.

Associated with pore structure analyses, the DMDS adsorption capacity is positively correlated with the specific surface area and pore volume, confirming the tunability of pore characteristics on adsorption performance via a well-controlled reduction procedure. These results highlight the significantly enhanced DMDS adsorption capacity for modified Cu-BTC samples with both suitable Cu(I)/Cu(II) molar ratio and tuned pore structures enabled by well-controlled reduction of Cu(II) to Cu(I) using $Na_2S_2O_3$.

3.3. Enhanced Adsorption Diffusion of DMDS on Cu-BTC. Furthermore, we determined the effects of $Na_2S_2O_3$ modification on adsorption diffusion of DMDS by conducting batch adsorption uptake experiment on the original and modified Cu-BTC samples. The adsorption uptake curve of DMDS of each Cu-BTC sample was measured at 288, 298, and 308 K (see Figure 10). All uptake profiles were fitted using an adsorption kinetic model (eq 2). The fitting results are shown in Figure 10. The derived adsorption kinetic parameters are further summarized in Table S5. The high correlation coefficients (R^2) indicate successful fitting for the experimental adsorption uptake data. According to Table S5, the modified Cu-BTC samples show higher diffusion coefficients (ranging from 3.40×10^{-13} to 5.14×10^{-13} cm^2/s at 288 K, 4.78×10^{-13} to 7.59×10^{-13} cm^2/s at 298 K, and 8.46×10^{-13} to 10.63×10^{-13} cm^2/s at 308 K) than the parent sample (2.92×10^{-13} cm^2/s at 288 K, 3.29×10^{-13} cm^2/s at 298 K, and 4.24×10^{-13} cm^2/s at 308 K). This strongly suggests that the rate of adsorption can be significantly enhanced through the postsynthesis modification using $Na_2S_2O_3$. Moreover, the Cu-BTC samples modified with $Na_2S_2O_3$ exhibit faster adsorption rate compared with the Cu-BTC samples modified using the EtOH/Ag system, with D of 4.73×10^{-13} cm^2/s at 298 K for DMDS adsorption on the Ag(0.10)/Cu-BTC/90%E sample.[41] Indeed, according to the SEM images, the uniform nanoscale pores observed on the surface of modified Cu-BTC may play a critical role governing such diffusion process, and the number of nanoscale pores is found to increase as the reduction time increases. In contrast, the absence of nanoscale porosity for either the parent Cu-BTC or the Ag(0.10)/Cu-BTC/90%E sample leads to poor molecular transport process. Therefore, controllable reduction of the Cu species in Cu-BTC using $Na_2S_2O_3$ results in increased capacity and higher diffusion rate for DMDS adsorption. This simple strategy has promising potential to greatly enhance the performance of adsorption removal of DMDS using Cu-BTC-based MOF materials.

3.4. DFT Calculations. DFT calculations were performed on DMDS adsorption on the parent and modified Cu-BTC structure models to reveal the mechanism determining the interaction between host framework and guest molecule. A cluster model taken from the Cu-BTC framework (see Figure S1)[42] with cluster edge being closed by hydrogen was used for all calculations. All Cu atoms at the edge of the cluster were replaced by H atoms, and the length of the terminal O−H bonds were fixed to be 1.1 Å. Other atoms were allowed to relax in the optimization process of geometry to assure that the entire cluster system maintains its structural stability. DMDS molecules were also geometrically optimized before adsorption, which were initially placed directly at the metal sites in each simulation. The distance between metal ions and adsorption sites was set to be 0.5 nm. Using the model structure proposed in our previous work[27] (see Figure S2), we replaced half of Cu(II) species with Cu(I) to represent the modified Cu(I)/Cu(II)-BTC structure. Adsorption configurations of DMDS on two cluster models (Cu(II)-BTC and

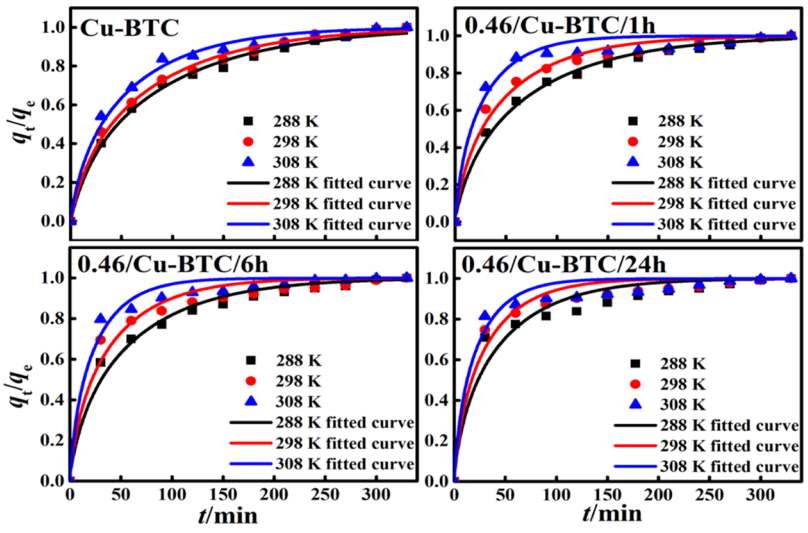

Figure 10. Adsorption uptake curves of DMDS on Cu-BTC samples modified with different reduction time (points: experimental values, lines: fitting results kinetic model).

DOI: 10.1021/acs.iecr.9b04349
Ind. Eng. Chem. Res. 2019, 58, 19503−19510

Cu(I)/Cu(II)-BTC) are presented in Figure 11. DMDS adsorption leads to much higher interaction energy on the

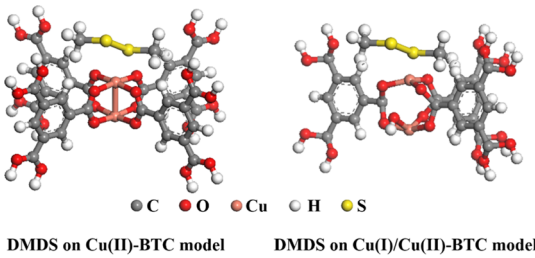

Figure 11. Adsorption configurations of DMDS on Cu(II)-BTC and Cu(I)/Cu(II)-BTC structure models.

modified Cu(I)/Cu(II)-BTC structure (70.65 kJ/mol) than on the parent Cu(II)-BTC (20.28 kJ/mol). Moreover, Mayer bond order (MBO) is used to evaluate the stability of bond in adsorption model. The structure with larger MBO tends to be more stable.[43] Compared with Cu(II)-BTC, Cu(I)/Cu(II)-BTC shows a slightly increased MBO from 0.5063 to 0.5543. An increase in MBO theoretically indicates stronger intermolecular binding, suggesting higher affinity for Cu(I)−DMDS interactions compared with Cu(II) species−DMDS interactions. This conclusion is supported by both experimental adsorption capacity data and interaction energy of the DFT calculation. The results in this study highlights that fine-tuned reduction of Cu(II) to Cu(I) using $Na_2S_2O_3$ leads to metal site oxidation state and pore structure modifications, which result in greatly enhanced DMDS adsorption capacity and diffusion on Cu-BTC.

4. CONCLUSIONS

In this study, we demonstrated that function modifications of Cu-BTC can be achieved via well-controlled reduction using $Na_2S_2O_3$. Compositional and structural evolutions of the modified samples upon reduction was examined using a variety of characterization techniques; the totality of the SEM, XRD, Raman, and XPS data indicate that long-range crystalline order is still retained even when a substantial fraction of the Cu(II) sites have been reduced via a fine-tuned reduction of Cu(II) to Cu(I). In addition, their DMDS adsorption performance was thoroughly evaluated. Specifically, among all samples, 0.46/Cu-BTC/24h with a Cu(I)/Cu(II) molar ratio of 1.79 exhibits the highest capacity (146.66 mg-S/g) and the fastest diffusion for DMDS adsorption ($D = 7.59 \times 10^{-13}$ cm^2/s at 298 K). DFT calculations indicate that the modified Cu(I)/Cu(II)-BTC structure has much stronger interactions with DMDS (70.65 kJ/mol) compared with the parent Cu(II)-BTC (20.28 kJ/mol). Such remarkable performance enhancement in both DMDS adsorption capacity and diffusion owing to controllable reduction of Cu(II) to Cu(I) using $Na_2S_2O_3$ will enable better adsorption removal of sulfides from mixtures using Cu-BTC-based materials. Moreover, our study provides a new method to modify MOFs materials for better performance as functional porous materials.

■ ASSOCIATED CONTENT

Supporting Information

The Supporting Information is available free of charge on the ACS Publications website at DOI: 10.1021/acs.iecr.9b04349.

Cu-BTC framework structure, structural evolution of Cu-BTC during reduction, convergence tolerance value for geometry optimization, postsynthesis conditions, XPS analysis results, pore structure analysis results, and kinetics parameters for adsorption of DMDS on Cu-BTC samples (PDF)

■ AUTHOR INFORMATION

Corresponding Authors

*E-mail: sunhui@ecust.edu.cn (H.S.).
*E-mail: d.wu@wsu.edu (D.W.).

ORCID

Hui Sun: 0000-0002-8544-756X
Jichang Liu: 0000-0002-5295-1778
Di Wu: 0000-0001-6879-321X

Notes

The authors declare no competing financial interest.

■ ACKNOWLEDGMENTS

This work is financially supported by the National Natural Science Foundation of China (grant 91634112 and 21878097), the Natural Science Foundation of Shanghai (grant 16ZR1408100), and the Open Project of State Key Laboratory of Chemical Engineering (SKL-ChE-16C01). Di Wu acknowledges the fund of Alexandra Navrotsky Institute for Experimental Thermodynamics, and the institutional funds from the Gene and Linda Voiland School of Chemical Engineering and Bioengineering at Washington State University.

■ ABBREVIATIONS

MOF	metal−organic framework
DMDS	dimethyl disulfide
SEM	scanning electron microscopy
XRD	X-ray powder diffraction
FTIR	Fourier transform infrared spectroscopy
XPS	X-ray photoelectron spectroscopy
DFT	density functional theory
PBE	Perdew−Burke−Ernzerhof
GGA	generalized gradient approximation
DSPP	DFT semicore pseudopods
DNP	double numerical basis sets plus polarization function
MBO	Mayer bond orders

■ REFERENCES

(1) Babich, I.; Moulijn, J. A. Science and technology of novel processes for deep desulfurization of oil refinery streams: a review. *Fuel* **2003**, *82*, 607.

(2) Mei, H.; Mei, B. W.; Yen, T. F. A new method for obtaining ultra-low sulfur diesel fuel via ultrasound assisted oxidative desulfurization. *Fuel* **2003**, *82*, 405.

(3) Tsai, C.; Li, H.; Park, S.; Park, J.; Han, H. S.; Nørskov, J. K.; Zheng, X. L.; Abild-Pedersen, F. Electrochemical generation of sulfur vacancies in the basal plane of MoS_2 for hydrogen evolution. *Nat. Commun.* **2017**, *8*, 15113.

(4) Wang, X.; Tang, Y.; Shi, P.; Fan, J.; Xu, Q.; Min, Y. Self-evaporating from inside to outside to construct cobalt oxide nanoparticles-embedded nitrogen-doped porous carbon nanofibers for high-performance lithium ion batteries. *Chem. Eng. J.* **2018**, *334*, 1642.

(5) Zinder, S. H.; Brock, T. D. Production of methane and carbon dioxide from methane thiol and dimethyl sulphide by anaerobic lake sediments. *Nature* **1978**, *273*, 226.

DOI: 10.1021/acs.iecr.9b04349
Ind. Eng. Chem. Res. 2019, 58, 19503−19510

(6) Ted Oyama, S. Novel catalysts for advanced hydroprocessing: Transition metal phosphides. *J. Catal.* **2003**, *216*, 343.
(7) Otsuki, S.; Nonaka, T.; Takashima, N.; Qian, W. H.; Ishihara, A.; Imai, T.; Kabe, T. Oxidative Desulfurization of Light Gas Oil and Vacuum Gas Oil by Oxidation and Solvent Extraction. *Energy Fuels* **2000**, *14*, 1232.
(8) Chan, N. Y.; Lin, T. Y.; Yen, T. F. Superoxides: Alternative Oxidants for the Oxidative Desulfurization Process. *Energy Fuels* **2008**, *22*, 3326.
(9) Gray, K. A.; Pogrebinsky, O. S.; Mrachko, G. T.; Xi, L.; Monticello, D. J.; Squires, C. H. Molecular mechanisms of biocatalytic desulfurization of fossil fuels. *Nat. Biotechnol.* **1996**, *14*, 1705.
(10) Roman, P.; Veltman, R.; Bijmans, M. F. M.; Keesman, K. J.; Janssen, A. J. H. Effect of Methanethiol Concentration on Sulfur Production in Biological Desulfurization Systems under Haloalkaline Conditions. *Environ. Sci. Technol.* **2015**, *49*, 9212.
(11) Pan, J.; Sun, Y.; Li, W.; Knight, J.; Manthiram, A. A green lead hydrometallurgical process based on a hydrogen-lead oxide fuel cell. *Nat. Commun.* **2013**, *4*, 2178.
(12) Hu, X.; Lu, Y.; Dai, F.; Liu, C.; Liu, Y. Host-guest synthesis and encapsulation of phosphotungstic acid in MIL-101 via "bottle around ship": An effective catalyst for oxidative desulfurization. *Microporous Mesoporous Mater.* **2013**, *170*, 36.
(13) Mostafa, M. S.; Betiha, M. A.; Rabie, A. M.; Hassan, H. M.; Morshedy, A. S. New Conduct in the Adsorptive Removal of Sulfur Compounds by New Nickel−Molybdenum Adsorbent. *Ind. Eng. Chem. Res.* **2018**, *57*, 425.
(14) Yan, Y.; Yang, S.; Blake, A. J.; Schröder, M. Studies on Metal-Organic Frameworks of Cu(II) with Isophthalate Linkers for Hydrogen Storage. *Acc. Chem. Res.* **2014**, *47*, 296.
(15) Wang, X.; Wu, W.; Chen, Z. L.; Wang, R. H. Bauxite-supported Transition Metal Oxides: Promising Low-temperature and SO_2-tolerant Catalysts for Selective Catalytic Reduction of NOx. *Sci. Rep.* **2015**, *5*, 9766.
(16) Dehghan, R.; Anbia, M. Zeolites for Adsorptive desulfurization from fuels: A review. *Fuel Process. Technol.* **2017**, *167*, 99.
(17) Coumans, A. E.; Poduval, D. G.; van Veen, J. A. R.; Hensen, E. J. M. The nature of the sulfur tolerance of amorphous silica-alumina supported NiMo(W) sulfide and Pt hydrogenation catalysts. *Appl. Catal., A* **2012**, *411−412*, 51.
(18) Seo, P. W.; Bhadra, B. N.; Ahmed, I.; Khan, N. A.; Jhung, S. H. Adsorptive Removal of Pharmaceuticals and Personal Care Products from Water with Functionalized Metal-organic Frameworks: Remarkable Adsorbents with Hydrogen-bonding Abilities. *Sci. Rep.* **2016**, *6*, 34462.
(19) Xu, Y.; Li, Q.; Xue, H.; Pang, H. Metal-Organic Frameworks for Direct Electrochemical Applications. *Coord. Chem. Rev.* **2018**, *376*, 292.
(20) Wu, L.; Xiao, J.; Wu, Y.; Xian, S.; Miao, G.; Wang, H.; Li, Z. A combined experimental/computational study on the adsorption of organosulfur compounds over metal-organic frameworks from fuels. *Langmuir* **2014**, *30*, 1080.
(21) Pearson, R. G. Hard and soft acids and bases. *J. Am. Chem. Soc.* **1963**, *85*, 3533.
(22) Hernández-Maldonado, A. J.; Yang, R. T. New sorbents for desulfurization of diesel fuels via π-complexation. *AIChE J.* **2004**, *50*, 791.
(23) Shi, R.-H.; Fan, H.-L.; Zhang, Z.-R.; Zhen, T.; Shangguan, J.; Mi, J. Cu-Based Metal−Organic Framework/Activated Carbon Composites for Sulfur Compounds Removal. *Appl. Surf. Sci.* **2017**, *394*, 394.
(24) Seredych, M.; Deliyanni, E.; Bandosz, T. J. Role of microporosity and surface chemistry in adsorption of 4,6-dimethyldibenzothiophene on polymer-derived activated carbons. *Fuel* **2010**, *89*, 1499.
(25) Seredych, M.; Bandosz, T. J. Removal of dibenzothiophenes from model diesel fuel on sulfur rich activated carbons. *Appl. Catal., B* **2011**, *106*, 133.
(26) Du, L.; Yang, J.; Xu, X. Highly enhanced adsorption of dimethyl disulfide from model oil on MOF-199/attapulgite composites. *Ind. Eng. Chem. Res.* **2019**, *58*, 2009.
(27) Sun, H.; Han, X.; Liu, K.; Shen, B.; Liu, J.; Wu, D.; Shi, X. Metal-Modified Cu-BTC Acid for Highly Enhanced Adsorption of Organosulfur Species. *Ind. Eng. Chem. Res.* **2017**, *56*, 9541.
(28) Ma, L.-P.; Dai, H.-B.; Liang, Y.; Kang, X.-D.; Fang, Z.-Z.; Wang, P.-J.; Wang, P.; Cheng, H.-M. Catalytically Enhanced Hydrogen Storage Properties of $Mg(NH_2)_2$ + 2LiH Material by Graphite-Supported Ru Nanoparticles. *J. Phys. Chem. C* **2008**, *112*, 18280.
(29) Kondo, S.; Ishikawa, T.; Abe, I.; Li, G. X. *Adsorption Science*, 2nd ed.; Chemical Industry Press: Beijing, 2005; p 31.
(30) Wu, X.; Ray, A. K. Density-functional study of water adsorption on the PuO_2(110) surface. *Phys. Rev. B: Condens. Matter Mater. Phys.* **2002**, *65*, 085403.
(31) Daniel Boese, A.; Chandra, A.; Martin, J. M. L.; Marx, D. From ab initio quantum chemistry to molecular dynamics: The delicate case of hydrogen bonding in ammonia. *J. Chem. Phys.* **2003**, *119*, 5965.
(32) Saraf, M.; Rajak, R.; Mobin, S. M. A Fascinating Multitasking Cu-MOF/rGO Hybrid for High Performance Supercapacitors and Highly Sensitive and Selective Electrochemical Nitrite Sensors. *J. Mater. Chem. A* **2016**, *4*, 16432.
(33) Erdem, B.; Hunsicker, R. A.; Simmons, G. W.; Sudol, E. D.; Dimonie, V. L.; EI-Aasser, M. S. XPS and FTIR surface characterization of TiO_2 particles used in polymer encapsulation. *Langmuir* **2001**, *17*, 2664.
(34) Petit, C.; Burress, J.; Bandosz, T. J. The synthesis and characterization of copper-based metal-organic framework/graphite oxide composites. *Carbon* **2011**, *49*, 563.
(35) Kaya-Celiker, H.; Mallikarjunan, P. K.; Kaaya, A. Characterization of Invasion of GenusAspergilluson Peanut Seeds Using FTIR-PAS. *Food Anal. Methods* **2016**, *9*, 105.
(36) Melo, R. S.; Silva, F. C.; Moura, K. R. M.; de Menezes, A. S.; Sinfrônio, F. S. M. Magnetic ferrites synthesized using the microwave-hydrothermal method. *J. Magn. Magn. Mater.* **2015**, *381*, 109.
(37) Prestipino, C.; Regli, L.; Vitillo, J. G.; Bonino, F.; Damin, A.; Lamberti, C.; Zecchina, A.; Solari, P. L.; Kongshaug, K. O.; Bordiga, S. Local Structure of Framework Cu(II) in HKUST-1 Metalorganic Framework: Spectroscopic Characterization upon Activation and Interaction with Adsorbates. *Chem. Mater.* **2006**, *18*, 1337.
(38) Dhumal, N. R.; Singh, M. P.; Anderson, J. A.; Kiefer, J.; Kim, H. J. Molecular Interactions of a Cu-Based Metal-Organic Framework with a Confined Imidazolium-Based Ionic Liquid: A Combined Density Functional Theory and Experimental Vibrational Spectroscopy Study. *J. Phys. Chem. C* **2016**, *120*, 3295.
(39) Vargas Jentzsch, P.; Kampe, B.; Rösch, P.; Popp, J. Raman Spectroscopic Study of Crystallization from Solutions Containing $MgSO_4$ and Na_2SO_4: Raman Spectra of Double Salts. *J. Phys. Chem. A* **2011**, *115*, 5540.
(40) Le, X. T.; Viel, P.; Sorin, A.; Palacin, S.; Jegou, P. Electrochemical behavior of polyacrylic acid coated gold electrodes: An application to remove heavy metal ions from wastewater. *Electrochim. Acta* **2009**, *54*, 6089.
(41) Han, X. *Study on Synthesis of MOF and Its Performance for Removing Organosulfurs from Light Hydrocarbons*; East China University of Science and Technology, 2018.
(42) Xiang, S.; Zhou, W.; Gallegos, J. M.; Liu, Y.; Chen, B. L. Exceptionally High Acetylene Uptake in a Microporous Metal-Organic Framework with Open Metal Sites. *J. Am. Chem. Soc.* **2009**, *131*, 12415.
(43) Zhu, H.; Guo, W.; Shen, Z.; Tang, Q.; Ji, W.; Jia, L. QSAR models for degradation of organic pollutants in ozonation process under acidic condition. *Chemosphere* **2015**, *119*, 65.

DOI: 10.1021/acs.iecr.9b04349
Ind. Eng. Chem. Res. 2019, 58, 19503−19510